Generative Model for the Inverse Design of Metasurfaces

Zhaocheng Liu,[†] Dayu Zhu,[†] Sean P. Rodrigues,[†,‡] Kyu-Tae Lee,[†] and Wenshan Cai*[,†,‡]

[†]School of Electrical and Computer Engineering and [‡]School of Materials Science and Engineering, Georgia Institute of Technology, Atlanta, Georgia 30332

S Supporting Information

ABSTRACT: The advent of metasurfaces in recent years has ushered in a revolutionary means to manipulate the behavior of light on the nanoscale. The design of such structures, to date, has relied on the expertise of an optical scientist to guide a progression of electromagnetic simulations that iteratively solve Maxwell's equations until a locally optimized solution can be attained. In this work, we identify a solution to circumvent this conventional design procedure by means of a deep learning architecture. When fed an input set of customer-defined optical spectra, the constructed generative network generates candidate patterns that match the on-demand spectra with high fidelity. This approach reveals an opportunity to expedite the discovery and design of metasurfaces for tailored optical responses in a systematic, inverse-design manner.

KEYWORDS: *Metasurface, nanophotonics, inverse design, neural networks*
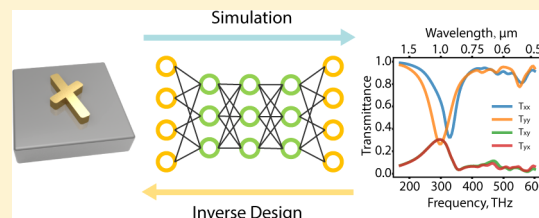
Close of the last century, discoveries in light-matter interactions on the nanoscale unlocked optical phenomena that would help to confine light to subwavelength scales, opening a gateway to a new era of optical design. The metasurfaces, a member of this family of new nanophotonic devices, is capable of generating periodic dipoles in order to manipulate the behavior of light in a nonclassically predicted manner. As such, a well-designed metasurface can tailor the transmittance and phase delay of electromagnetic waves over any wavelength spectrum.[1−5] The realization of these materials has led to a vast number of applications in perfect absorption,[6] super resolution imaging,[7,8] beam steering,[9,10] and nonlinear optical generation.[11,12]

As these nanostructured materials require labor intensive fabrication, an accurate prediction of the optical spectrum and structure of the envisioned metasurfaces must be preemptively articulated. However, the complicated physical mechanisms that describe these light-matter interactions at the nanoscale cannot be resolved by generalized theory and as such the prediction of a material's optical properties and approximate structure relies on advanced iterative calculations achieved by finite-element modeling (FEM) or finite-difference time-domain (FDTD) methods. Moreover, this conventional metasurface design process is innately flawed by human guided error. Not only is the initial design realized based on physical insights and intuitive reasoning, but the finalized geometric and material parameters are ultimately achieved by a means of trial-and-error. The design of such optical systems demands a working knowledge base of optics in order to moderate iterative simulations that scan multidimensional parameter spaces. Thanks to rapid developments in artificial intelligence (AI), some scientific problems that classically required human perception or intricate mechanisms have recently been solved by AI.[13−17] Such methods have translated into the field of

optics, by employing optimization methods[18−23] and evolutionary algorithms[24] to expedite the design of photonic devices. To accelerate the design process without extensive computation (numerical or analytical) of Maxwell's equations, data driven methods, especially deep neural networks, have been gradually incorporated into the design of microwave and nanophotonics devices.[25−28]

With growing interest of new phenomena and applications using metasurfaces, there is an ever-pressing need to develop efficient methods that expedite the discovery and design of novel metasurface structures with custom-defined functionality. As illustrated in Figure 1a, this work aims to leverage deep neural networks to approximate the spectra of a metasurface and, more importantly, to generate metasurface patterns that yield customer-defined spectra at the input. The latter is the long-sought-after goal of inverse optical design in which a working structure is to be generated directly based on the desired optical responses of the designer. In doing so, the need for extensive parameter scans or trial-and-error procedures is bypassed. However, due to the enormous degrees of freedom in typical metasurface patterns, conventional neural network schema, like backpropagation in trained simulator networks,[28] are impotent in the inverse design of metasurfaces. In addition, the trained simulator defines the problem as a deterministic system, such that a single simulator will inevitably lead to a fixed outcome for a given input condition. Meanwhile, multiple solutions may exist for the same target spectrum fed to the simulator at the input, thereby imposing an unnecessary constraint on the diversity of the optimized structures.
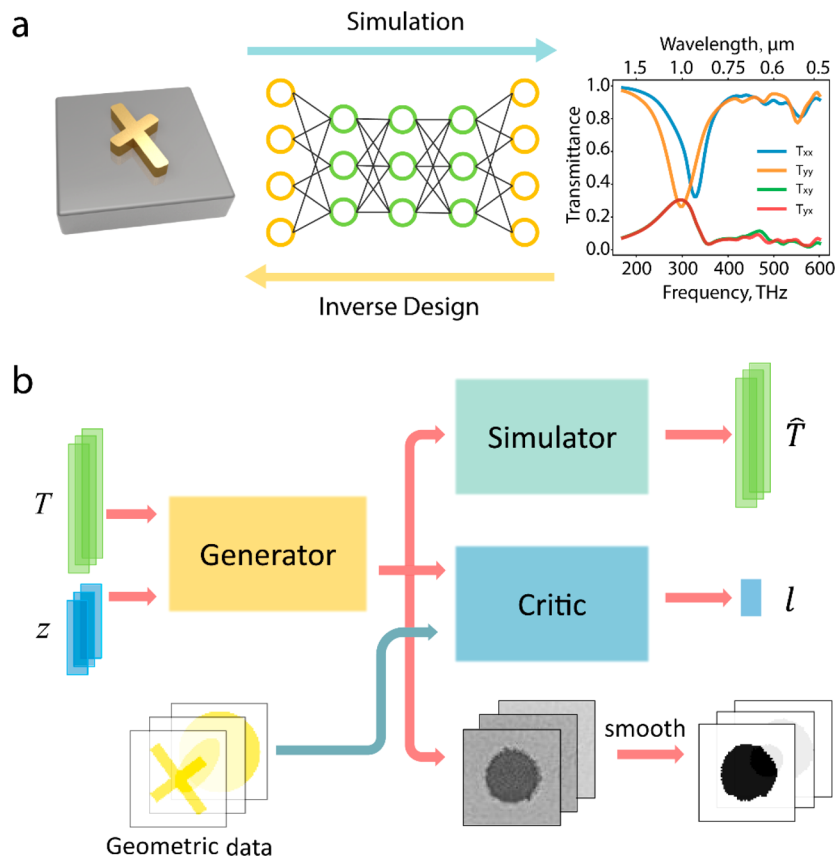
Figure 1. Transitioning metasurface design from conventional trial-and-error approaches to neural network mediated inverse design. (a) Both simulation and inverse design enact structure—property relationships to generate an optical spectrum from a metasurface and vice versa. In this work, both processes will be replaced by deep neural networks. (b) Architecture of the proposed network for AI-based optical design. Three networks, the generator, the simulator, and the critic constitute the complete architecture. The generator accepts the spectra T and noise z and produces possible patterns. The simulator is a pretrained network that approximates the transmittance spectrum $\hat{T}$ for a given pattern at its input, and the critic evaluates the distance of the distributions between the geometric data and the patterns from the generator. While training the generator, the produced patterns vary according to the feedback obtained from S and D. Valid patterns are documented during the training process, and are smoothed to qualify as candidate structures.

To mitigate these challenges, here we adopt a generative adversarial network (GAN) in the network model. A GAN is an unsupervised learning architecture consisting of two networks, namely a generator and a critic, that contesting with each other to create authentic image and video data sets.[29−32] Instead of employing a single simulator to tackle the inverse design problem, we incorporate a GAN to jointly seek the structures for the intended spectra at the input. We have also constructed a geometric data set that is comprised of images of random shapes. When training the GAN-based network with the geometric data, the resultant patterns from the network will resemble some samples in the geometric data set. Because constructing such geometric data is largely effortless, given a sufficiently large data set of the geometries we will be able to identify and refine proper shapes of the structures in order to replicate the demanded spectra at the input of the networks. Compared to existing practices of optical design with neural networks, which are only able to optimize a few geometrical parameters of a fixed structure represented as vectors (i.e., thickness distribution of layered systems), our network allows for the generation of essentially arbitrary patterns of the unit cell structure, represented as pixelwise images. In contrast to deterministic optimization approaches, which achieve one suboptimum nanostructure after expensive computation of Maxwell's equations, our

approach allows one to avoid local minimum by identifying multiple patterns with distinct topologies in a short period of time. Moreover, the technique developed here can process multiple input spectra in parallel, which facilitates efficient design and optimization of more than one optical structures simultaneously. Such a need is commonly encountered in metasurfaces research, where gradient metastructures of varying unit cells are distributed in a two-dimensional space for wavefront shaping applications such as metaholograms, vortex generation, and planar lenses.

Network Architecture. To realize the AI-based optical design described above, we have constructed a network architecture as illustrated Figure 1b. We divide the network into three parts: a simulator (S), a generator (G), and a critic (D). The primary goal is to train an overfitted generator, which produces metasurface patterns in response to given input spectra T such that the Euclidean distance between the spectra of the generated pattern T' and the input spectra T is minimized. All three networks are convolutional neural networks with delicate differences in detailed structures. The simulator is a pretrained model with fixed weights, taking the generated patterns as input and approximating their transmittances spectra $\hat{T}$ without the use of electromagnetic simulations. It is built to control the accuracy of the optical spectra of the generated structures when training the generator.
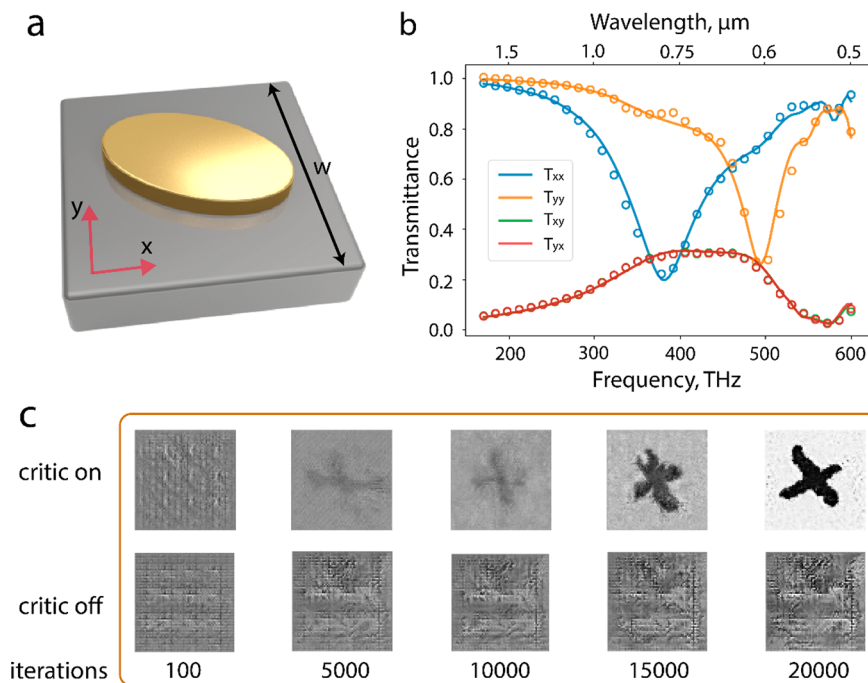
Figure 2. Effectiveness of the engineered simulator and critic networks. (a) The unit cell of the metasurface used in our case study of the inverse design problem. The pattern is allowed to vary for a desired spectral response with the following structural and material constraints enforced: gold for the pattern and glass as the substrate; unit cell size w = 340 nm; thickness of gold d = 50 nm. (b) Transmission spectra of a representative structure shown in (a), obtained by FEM electromagnetic simulation (solid lines) and by the simulator network (circles), respectively. (c) Generated patterns during the training process after certain iterations with and without the critic network. Only geometric data categorized as a cross are fed into the critic in this example.

The generator and the critic together constitute a GAN. The critic of this GAN accepts both the user-defined geometric data and the patterns generated from the generator, and then yields a value l which is essential to compute the distance between the distributions of the two sets of data. By minimizing this distance, the critic network guides the generator to produce patterns that share commons features with the input geometric data. During the training process, we update the weights in the generator by backpropagation from the losses defined by the simulator and the critic. Valid patterns produced by the generator are documented throughout the training process; this occurs whenever the losses of the simulator and critic are sufficiently small. The generated patterns are finally smoothed to binary images as candidates of the metasurface design. Detailed network configurations and training methods are presented in the Supporting Information.

In essence, the critic learns the distribution of the geometric data and restricts the generator to produce patterns in the image space in which the geometric data resides. Although it is mathematically possible to define a function to replace the critic network, it is unfeasible to identify an explicit expression for the function when the geometric data are diverse and complicated as seen in our case. There are several benefits of including such a network critic into the overall network architecture. First, it excludes a large number of unacceptable patterns that are deemed unrealistic in actual nanofabrication. Second, it allows us to control the overall shape of the generated patterns by feeding similar geometries into the critic. While such forethoughts are not necessary for AI-guided optical design, as demonstrated in the latter part of this work, certain geometrical constraints at the input may help to narrow down the potential candidates and thereby expedite the

convergence to a solution. Finally, because the production of various categories of geometric data is straightforward and largely effortless, we can modify the distributions of the geometric data to avoid degeneracy. This may occur when multiple metasurface patterns of different topologies possess identical optical spectra to the input spectra within an acceptable margin of deviation.

As a representative and generalizable case study, we will apply the strategy outlined above to the design of metasurfaces with prescribed spectral behavior under linearly polarized illumination. The general unit cell of the metasurface used in this model is shown in Figure 2a, which has a single layered gold pattern in a square lattice, situated on a glass substrate. Other common parameters include a lattice constant of w = 340 nm and a thickness of the gold layer set to d = 50 nm. To train the simulator with sufficient data, we carried out 6500 full wave finite element method (FEM) simulations for metasurfaces with a wide variety of shapes that replaced the metal in the unit cells. The simulation was run over a frequency span from f = 170−600 THz (i.e., 500 nm to 1.8 μm in the wavelength domain), which covers a major portion of the visible and the near-infrared spectral range. These FEM simulations yield the transmittance magnitude spectra T_{ij} of each metasurface under x- and y-polarized illumination, where i and j indicates the polarization directions for the incidence and the detection, respectively. Throughout the training, the unit cell structure is represented as a binary image of 64 × 64 pixels, in which 1 stands for gold and −1 for void (air). Each transmission spectrum $T_{ij}(f)$ is represented as a 32-entry vector with equal frequency intervals. The simulator after the training process is able to approximate the transmittance T with an average absolute error of less than 0.01 at each
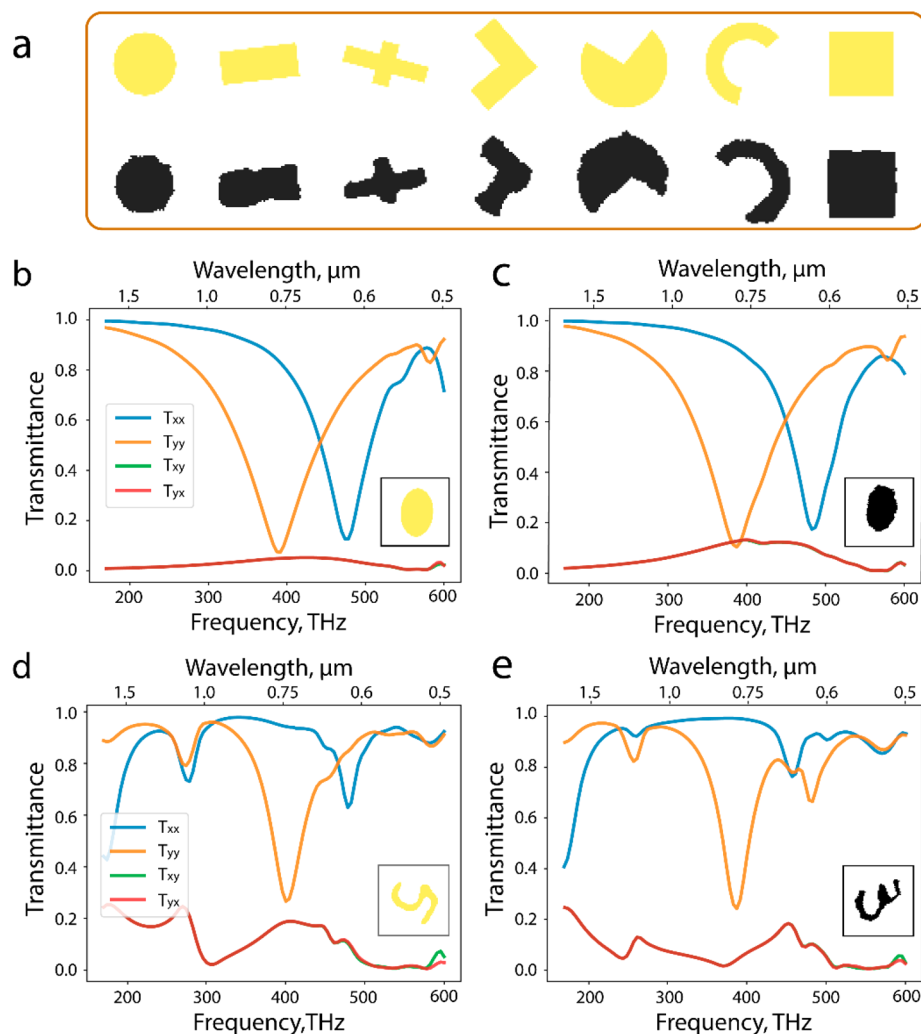
Figure 3. Generating patterns with a predesigned class of geometric data. (a) Test patterns s are depicted in the top row and the corresponding generated patterns s' are listed in the bottom row. Each shape provides a sample of the different classes of geometric data input to the critic network. (b) Transmittance spectra, T', of a test pattern s, to be fed to the network. (c) FEM simulated transmittance of the retrieved pattern s', from the neural network based on the input as in (b). The unit cells of s and s' are shown in the lower right corner of each figure. This result is achieved when the critic only receives geometric data of the elliptical class. (d,e) An example of results with a modified MNIST handwritten digital data set as the input geometric data. Note that in this experiment, we intentionally excluded digit "5" in the input geometric data.

frequency point. An example for the effectiveness of the simulator is illustrated in Figure 2b, where the solid lines are the results from the FEM electromagnetic simulations for the ellipse particle array shown in Figure 2a. Here, the circles represent the spectral approximation of the same structure obtained by the neural network.

To demonstrate the mechanism and performance of the network, we classify the geometric data into several classes such as circles, arcs, crosses, ellipses, rectangles, and so forth. A full list of the training data and corresponding samples are made available in the Supporting Information. Figure 2c illustrates a series of generated patterns during a training process after certain iterations, with and without the critic network. For this example, the critic is fed with a class of geometric data only comprised of crosses. When the critic is on, the generator receives feedback from the loss of both the simulator and the critic. A cross pattern emerges and gradually adjusts itself to meet the requirement of the input spectrum. In sharp contrast, when the critic network is turned off, the generator is then optimized to merely reduce the loss of the

simulator. Without the constraint enforced by the critic, the generated pattern becomes a cluster of random pixels and stays stabilized after a few hundred iterations. This comparison demonstrates the pivotal role of the critic in narrowing down the solution space to the interested region. The function of the critic in our proposed strategy largely resembles those used in GANs to handle the image generation tasks.

Results and Analysis. Our network architecture is capable of generating metasurface patterns in response to an arbitrarily input, on-demand set of optical spectra, whose T_{ij} components and frequency range of interest are defined by the user. At the input of the generator, we specify a set of transmittance spectra T_{ij} from 170 to 600 THz, which corresponds to a wavelength range of 500 nm to 1.8 μm. In the following discussion, we define a set of patterns to be used as a test set and denote this test set as s, the spectra of each s as T. Once these spectra are passed through the network architecture, a pattern is retrieved which we denote as s' in correspondence to s. In verification, the generated set s' is FEM-simulated and defined as T'. Unless mentioned otherwise, in the following experiments we
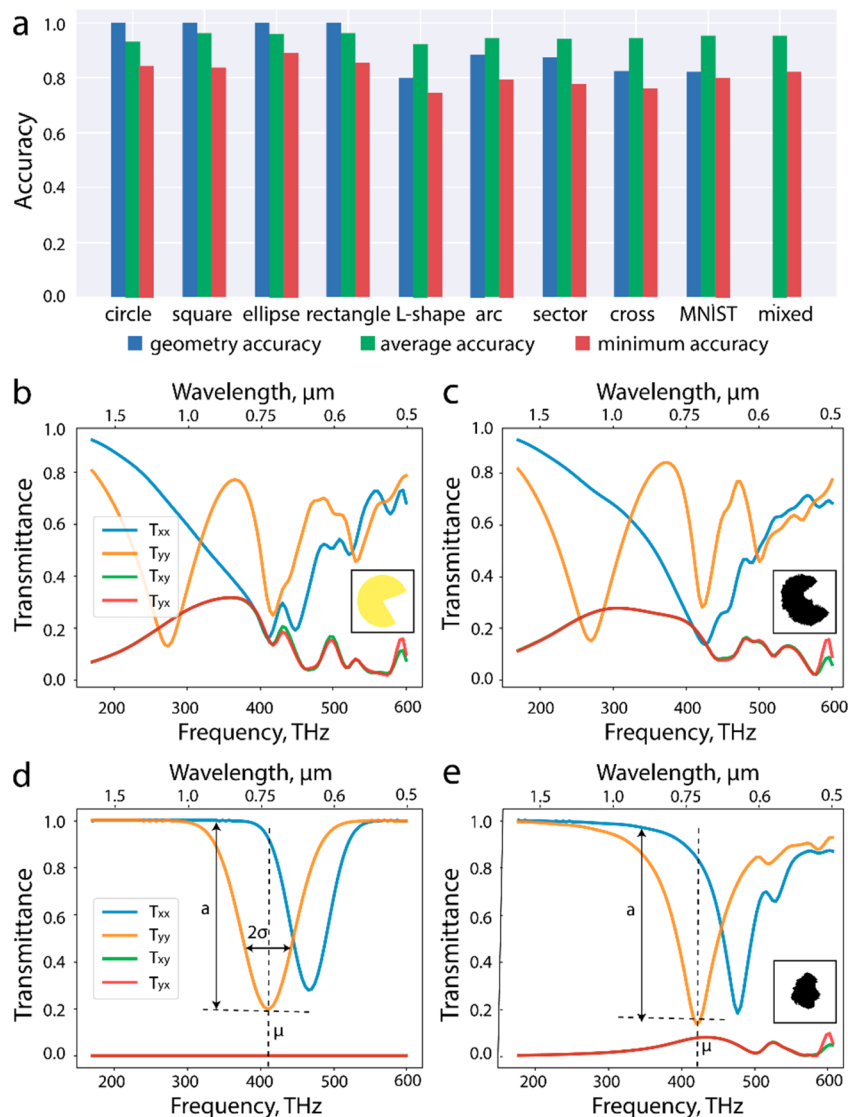
Figure 4. Statistical accuracy of the model and examples of generated patterns with mixed classes of geometric data. (a) Geometric accuracy, average accuracy, and minimum accuracy of experiments with the different classes of geometric data. (b,c) Example of results with a mixture of different classes of geometric data used at the input. Transmittance spectra of the test structure s and the generated pattern s' are shown in the (b) and (c), respectively, with the unit cell depicted as the inset in each figure. (d,e) Example of Inverse design of metasurfaces with human-defined spectra. (d) Desired transmittance spectra as the input to the generator, where T_{xx} and T_{yy} are two randomly generated Gaussian-like responses with parameters a, μ, and σ, while T_{xy} and T_{yx} are 0 throughout the frequency range of interest. (e) The resultant unit cell generated by our AI model to fit the target spectra, along with the FEM simulated transmittance spectra of this generated metasurface.

set the number of patterns being parallelly searched at each run to be 40 and the total iterations of the training to be 50 000. For each target spectrum, valid patterns may occur at different stages of the training process whenever the losses of the simulator and critic are both reasonably small. On a machine with a single GPU Quadro P5000, it takes approximately 10 min to carry out 10 000 iterations of training on average.

As an initial demonstration, to illustrate the overall competence of the proposed framework we use the spectra, T, of randomly selected test samples from each geometric class as the input and allow the network to seek proper patterns based on these spectra. In this situation, we ensure the existence of solutions by using actual spectra of real patterns as the "target" or input. This constraint will be removed when we perform the inverse design for on-demand spectra, as presented in a later part of the paper. In each test, the critic is fed with 1000 data points (i.e., geometrical shapes) that are

randomly generated from the same geometric class. Figure 3a shows representative samples from such experiments for each class of the geometry. The first row depicts the test samples s, and the second row shows the corresponding samples s' generated by the network. The geometric patterns in each pair of the two rows agree very well, partially because the full spectra input T_{ij} to the generator substantially narrows down the possible solutions. Because the generator does not receive any direct information on the geometry for the input spectra, it may uncover equivalent patterns s' that are different from the test structures s while yielding the same spectral behavior. Such examples can be found in the cross, sector and arc cases in Figure 3a, where the discovered patterns s' are mirror-flipped counterparts of s with the same optical responses under linearly polarized illuminations.

Figure 3b,c shows the spectra of an ellipse test sample s and those of the discovered pattern s' with the corresponding unit

cell of the metasurface placed as insets. Comparison between the two sets allows us to conclude that the network has successfully identified the correct structure to replicate the spectra with only minor deviations. We also note that the geometric data fed into the critic network does not necessarily contain the right shape of the resultant solutions. If the type of the right pattern s for the required spectra is contained in the geometric data at the input, the nature of the GAN will lead to a decent chance of identifying the structure s as a proper candidate; otherwise, the critic will guide the generator to produce patterns with geometric features similar to those of the right geometry.[29]

To illustrate the ability of our model to optimize structures of any shape, we further test our network with handwritten digit data set MNIST as the unit patterns of metasurfaces.[33] We modify patterns from the MNIST data set with rotation and shifting, and then feed them into the critic during the training. In this experiment, we intentionally exclude digit "5" in the geometric data set at the input of the critic, and ask the network to generate a pattern that replicates the spectral features of a metasurface with digit "5". Figure 3d,e shows the spectra of the test sample , a rotated digit "5", and the discovered pattern s', a modified digit "3", respectively. The topologies of the s and s' differ considerably, but the overall transmittance behaviors of the two samples, especially T_{xx} and T_{yy}, possess similar features in terms of both the spectral location and the amplitude. By removing the input structure from the trained data set, the network proves its overarching utility in producing a set of spectra that can competently match that of the input structure.

To quantify the performance of the network, we quantitatively define three types of accuracy as follows. (1) Geometric accuracy: the portion of s' that can be recognized as within the same class of the input geometric data. (2) Average accuracy $1 - e_{ave}$, where e_{ave} is the average absolute error of the transmittance per frequency point. (3) Minimum accuracy $1 - e_{max}$, where e_{max} represents the largest absolute error of the transmittance over all frequencies. Figure 4a displays the three accuracies in our experiments for various classes of geometry. The average and minimum accuracies are calculated based on the correct ones in s' in terms of the geometric accuracy. We also note that these accuracies are data-dependent and may vary when the distribution of geometric data changes.

Next, to further exemplify the generality and versatility of the constructed network, we feed into the critic mixed data from all classes of geometry with over 8000 data points, and the test samples are also randomly selected from all possible geometries. As shown in the last column of Figure 4a, the accuracy in this situation does not degrade compared to prior studies with only a single geometry input. An example of a discovered structure with mixed geometric input is presented in Figure 4b,c. Just as before, Figure 4b,c indicates the FEM-simulated spectra of the test pattern s and the generated pattern s' in response to the spectral demand, respectively. Although no specific class of geometry is indicated during the training, the generator is able to reach a pattern, s', that not only geometrically resembles s but more importantly possesses transmittance spectra, T', nearly identical to that of T. In general, if the input geometric data contains more than one topology that satisfies the spectral demand, the network may generate some or all of them in a probabilistic manner. Moreover, by changing the distribution of the geometric data, the user may achieve diverse solutions in response to the same

spectral request, thereby mitigating the potential of degeneracy, as described earlier.

As a final example, we demonstrate the efficacy of our approach in the reverse design of a metasurface for user drawn spectral responses, T. In practice, the desired spectra at the input are user defined, and the existence of solutions is not guaranteed. This is particularly true when certain constraints are applied to the metasurface design. For instance, in the present study parameters such as the materials used, the unit cell size, and the thickness of the patterned layer are all predefined in the training data. Nevertheless, when the simulator is sufficiently robust, the network is still able to unearth the best possible pattern that yields spectra T' with minimized deviation from the input spectra T. To demonstrate this feature, here we design a metasurface with the desired, user-defined spectra behavior shown in the Figure 4d: (i) T_{xx} and T_{yy} are two Gaussian-like resonances with randomly chosen mean μ, variance σ, and amplitude a, and (ii) T_{xy} and T_{yx} are zero. The generated pattern along with its spectra T' is shown in the Figure 4e. Although there exists no exact solution to spectral demand described above, the network eventually generates patterns whose spectra share common features with the input spectra including the resonance frequency, the spectral bandwidth, and the transmission magnitude.

Conclusion. In this work, we have proposed a generative, deep, network model which efficiently discovers and optimizes unit cell patterns of metasurfaces in response to user-defined, on-demand spectra at the input. Our model addresses the pursuit of reverse design technology for photonic structures and helps to relieve computational and specialist resources in traditional metasurface design from iterative simulations and parameter sweeping up to generalizing the process for users lacking a solid knowledge base in optics. The model developed here is mostly based on the unsupervised learning, which guarantees efficient generation of structural patterns independent of human experience. This feature is crucial in the investigation of new structures and novel phenomena in optics and beyond. In addition, as our model can process multiple input spectra without the loss of efficiency, the workload for complicated problems that require multiple metasurfaces or gradient structural distributions will be significantly reduced. The performance of the model can be further improved by applying certain refinements, such as the use of a more sophisticated network configuration and the introduction of loss functions with more practical physical meanings.

The methodology we have developed is readily extended to the pursuit of desired complex values of the reflection and transmission coefficients, which is essential to the applications like meta-lenses and meta-holograms where both the amplitude and the phase of the light waves matter. For example, by replacing the simulator used here with a more comprehensive simulator trained to approximate the spectra and phase delay of all-dielectric nanostructures, our approach can be adapted for the design of metasurfaces with prescribed intensity distribution and dispersion angle of light at arbitrary wavelengths. In the current work, we restrict the unit pattern of the metasurface as a single metallic particle with continuous topology. By revising the geometric data set and refining the simulator, unit cells with multiple particles and complicated structures can be designed and optimized as well. The increased arbitrariness of topology can significantly improve the spectral accuracy of the outcome from our model. Moreover, if sufficient data for the training of the simulator

is available, greater degrees of freedom in the design can be made by slightly modifying the network architecture to include modifications of the lattice constant or optimization of the pattern thickness. Further improvement in subsequent studies may include the incorporation of other AI algorithms, such as the reinforcement learning and the evolutionary algorithms, to mitigate the dependency of prior knowledge of human and alleviate the amount of data for the training. The developed framework can be adapted to many other applications in optics and materials science, including multilayer metasurfaces, photonic crystals, 3D metamaterials, imaging systems, phase transitions, and so forth. We envision broad and growing utilization of the deep learning technology in the physics realm so that scientists and engineers will be largely relieved from tedious processes of trial and error and instead focus more on truly creative thoughts yet to be broached by the machine.

■ ASSOCIATED CONTENT

Ⓢ Supporting Information

The Supporting Information is available free of charge on the ACS Publications website at DOI: 10.1021/acs.nano-lett.8b03171.

> Detailed information on the network architecture; algorithms and hyperparameters used in the training; post processing of the image; performance on partial input spectra; additional samples of results of the experiments in the main article; additional samples of results with manually defined input spectra; detailed information on the geometric data set; mathematical definitions of the geometric, average and minimum accuracy (PDF)

■ AUTHOR INFORMATION

Corresponding Author

*E-mail: wcai@gatech.edu.

ORCID Ⓘ

Wenshan Cai: 0000-0002-6367-3857

Notes

The authors declare no competing financial interest.

■ ACKNOWLEDGMENTS

■ REFERENCES

(1) Yu, N.; Capasso, F. *Nat. Mater.* **2014**, *13* (2), 139.

(2) Kildishev, A. V.; Boltasseva, A.; Shalaev, V. M. *Science* **2013**, *339* (6125), 1232009.

(3) Lin, D.; Fan, P.; Hasman, E.; Brongersma, M. L. *Science* **2014**, *345* (6194), 298−302.

(4) Chu, C. H.; Tseng, M. L.; Chen, J.; Wu, P. C.; Chen, Y. H.; Wang, H. C.; Chen, T. Y.; Hsieh, W. T.; Wu, H. J.; Sun, G.; Tsai, D. P. *Laser & Photonics Reviews* **2016**, *10* (6), 986−994.

(5) Silva, A.; Monticone, F.; Castaldi, G.; Galdi, V.; Alù, A.; Engheta, N. *Science* **2014**, *343* (6167), 160−163.

(6) Yao, Y.; Shankar, R.; Kats, M. A.; Song, Y.; Kong, J.; Loncar, M.; Capasso, F. *Nano Lett.* **2014**, *14* (11), 6526−6532.

(7) Larouche, S.; Tsai, Y.-J.; Tyler, T.; Jokerst, N. M.; Smith, D. R. *Nat. Mater.* **2012**, *11* (5), 450.

(8) Zheng, G.; Mühlenbernd, H.; Kenney, M.; Li, G.; Zentgraf, T.; Zhang, S. *Nat. Nanotechnol.* **2015**, *10* (4), 308.

(9) Pfeiffer, C.; Grbic, A. *Phys. Rev. Lett.* **2013**, *110* (19), 197401.

(10) Arbabi, A.; Horie, Y.; Bagheri, M.; Faraon, A. *Nat. Nanotechnol.* **2015**, *10* (11), 937−943.

(11) Butet, J.; Brevet, P.-F.; Martin, O. J. *ACS Nano* **2015**, *9* (11), 10545−10562.

(12) Li, G.; Chen, S.; Pholchai, N.; Reineke, B.; Wong, P. W. H.; Pun, E. Y. B.; Cheah, K. W.; Zentgraf, T.; Zhang, S. *Nat. Mater.* **2015**, *14* (6), 607.

(13) Carrasquilla, J.; Melko, R. G. *Nat. Phys.* **2017**, *13* (5), 431.

(14) Chen, Y.; Lin, Z.; Zhao, X.; Wang, G.; Gu, Y. *IEEE Journal of Selected Topics in Applied Earth Observations and Remote Sensing* **2014**, *7* (6), 2094−2107.

(15) Segler, M. H.; Preuss, M.; Waller, M. P. *Nature* **2018**, *555* (7698), 604.

(16) Poloni, C.; Giurgevich, A.; Onesti, L.; Pediroda, V. *Computer Methods in Applied Mechanics and Engineering* **2000**, *186* (2−4), 403−420.

(17) Melnikov, A. A.; Nautrup, H. P.; Krenn, M.; Dunjko, V.; Tiersch, M.; Zeilinger, A.; Briegel, H. J. *Proc. Natl. Acad. Sci. U. S. A.* **2018**, *115*, 1221.

(18) Lu, J.; Vučković, J. *Opt. Express* **2013**, *21* (11), 13351−13367.

(19) Piggott, A. Y.; Lu, J.; Lagoudakis, K. G.; Petykiewicz, J.; Babinec, T. M.; Vučković, J. *Nat. Photonics* **2015**, *9* (6), 374−377.

(20) Sitawarin, C.; Jin, W.; Lin, Z.; Rodriguez, A. W. *Photonics Res.* **2018**, *6* (5), B82−B89.

(21) Callewaert, F.; Velev, V.; Kumar, P.; Sahakian, A.; Aydin, K. *Sci. Rep.* **2018**, *8* (1), 1358.

(22) Lin, Z.; Groever, B.; Capasso, F.; Rodriguez, A. W.; Lončar, M. *Phys. Rev. Appl.* **2018**, *9* (4), 044030.

(23) Sell, D.; Yang, J.; Doshay, S.; Yang, R.; Fan, J. A. *Nano Lett.* **2017**, *17* (6), 3752−3757.

(24) Wiecha, P. R.; Arbouet, A.; Girard, C.; Lecestre, A.; Larrieu, G.; Paillard, V. *Nat. Nanotechnol.* **2016**, *12* (2), 163.

(25) Hoole, S. R. H. *IEEE Trans. Magn.* **1993**, *29* (2), 1931−1934.

(26) Kabir, H.; Wang, Y.; Yu, M.; Zhang, Q.-J. *IEEE Trans. Microwave Theory Tech.* **2008**, *56* (4), 867−879.

(27) Liu, D.; Tan, Y.; Khoram, E.; Yu, Z. *ACS Photonics* **2018**, *5* (4), 1365−1369.

(28) Peurifoy, J.; Shen, Y.; Jing, L.; Yang, Y.; Cano-Renteria, F.; DeLacy, B. G.; Joannopoulos, J. D.; Tegmark, M.; Soljačić, M. *Science Advances* **2018**, *4* (6), eaar4206.

(29) Goodfellow, I.; Pouget-Abadie, J.; Mirza, M.; Xu, B.; Warde-Farley, D.; Ozair, S.; Courville, A.; Bengio, Y. In *Generative adversarial nets*; Advances in Neural Information Processing Systems, Ghahramani, Z.; Welling, M.; Cortes, C.; Lawrence, N.D.; Weinberger, K. Q., Eds.; Curran Associates: Red Hook, NY, 2014; pp 2672−2680.

(30) Radford, A.; Metz, L.; Chintala, S. Unsupervised Representation Learning with Deep Convolutional Generative Adversarial Networks. arXiv preprint arXiv:1511.06434 **2015** (accessed Nov 19, 2015).

(31) Arjovsky, M.; Chintala, S.; Bottou, L. In *Wasserstein Generative Adversarial Networks*; International Conference on Machine Learning, Proceedings of the 34th International Conference on Machine Learning, Sydney, Australia, 2017; PMLR, Vol. 70, 214−223.

(32) Gulrajani, I.; Ahmed, F.; Arjovsky, M.; Dumoulin, V.; Courville, A. C. In *Improved Training of Wasserstein GANs*; Advances in Neural Information Processing Systems, Guyon, I.; Luxburg, U. V.; Bengio, S.; Wallach, H.; Fergus, R.; Vishwanathan, S.; Garnett, R., Eds.; Curran Associates: Red Hook, NY, 2017; pp 5769−5779.

(33) LeCun, Y.; Jackel, L.; Bottou, L.; Cortes, C.; Denker, J. S.; Drucker, H.; Guyon, I.; Muller, U.; Sackinger, E.; Simard, P. Learning algorithms for classification: A comparison on handwritten digit recognition, in *Neural Networks: The Statistical Mechanics Perspective*; Oh, J. H.; Kwon, C.; Cho, S., Eds.; World Scientific: Singapore, 1995, ,271−276.